Figure S1. Comparison of the co-registration accuracy in the (a) range and (b) Azimuth directions based on the digital elevation model (DEM) and coherence coefficient. Dark blue columns represent the residual offset standard deviation (SD) of the model based on the coherence coefficient. Red columns are the residual offset SD of the model based on the DEM. MR: mean SD in the range direction of the model based on the coherence coefficient; MRlt: mean SD in the range direction of the model based on the DEM; MAZ: mean SD in the Azimuth direction of the model based on the coherence coefficient; and MAZlt: mean SD in the Azimuth direction of the model based on the DEM.

We compared the co-registration based on the digital elevation model (DEM) and coherence coefficient and found that the accuracy of co-registration in the range direction was greatly improved, the mean standard deviation (SD) of residual offsets dropped from 0.22 to 0.13 (Figure 2a) and the accuracy in the azimuth direction was slightly improved (Figure 2b).
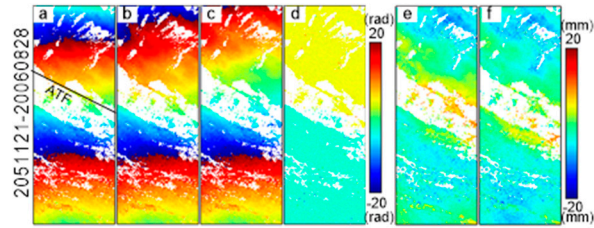

Figure S2. Interferogram showing the effects of atmospheric phase screen (APS) and DEM errors and the orbital ramp. (a) Observation interferogram; (b) APS-corrected interferogram; (c) DEM error-corrected interferogram; (d) Difference of (b) and (c), which was near to a constant; (e) without and (f) with unwrapping error correction.

In this study, we removed the atmospheric delay from the original observations (Figure S2a) and obtained an atmospheric phase screen (APS)-corrected interferogram (Figure S2b). Profiles a and b in Figure S3 show the phase quantification of the original and APS-corrected interferograms. The atmospheric delay was mostly reduced across the ATF. However, in the presence of steep topography, interpolating weather model parameters between grid nodes at significantly different elevations can produce artifacts in phase-delay maps because the weather model must be extrapolated below the Earth's surface. Artifacts were decreased by following local DEM error correction.
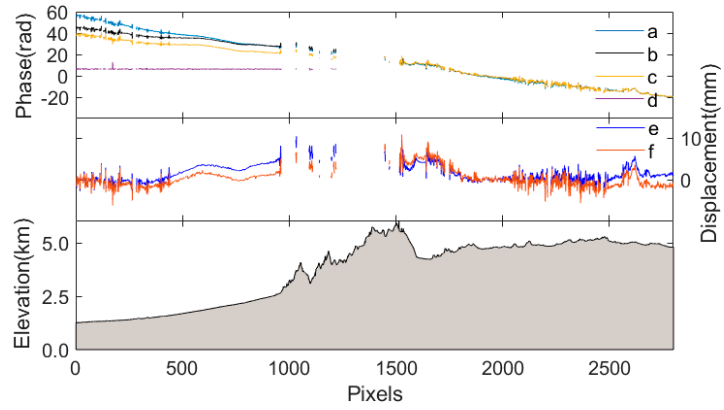
Figure S3. Profiles a, b, c, and d are the unwrapped phase of the middle row of interferograms a, b, c, and d, respectively, in Figure S2. The value of profile d is about 6.28 rad, which is one cycle or the phase step when unwrapping. Profiles e and f are the displacement of the middle row of interferograms e and f, respectively, in Figure S3. The gray profile is the elevation.
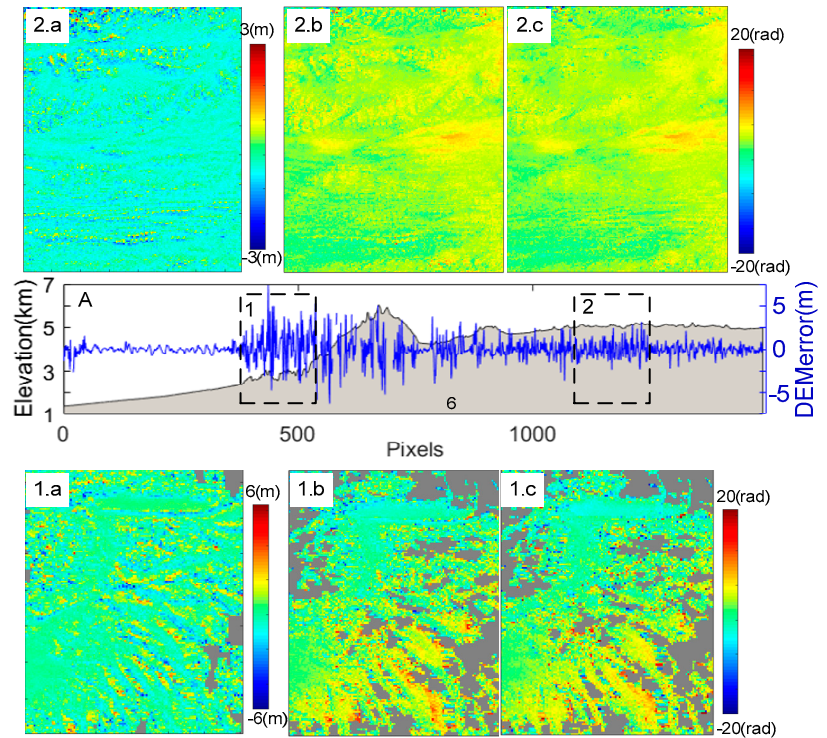

Figure S4. Profile of the DEM errors and elevation. The DEM error maps 1.a and 2.a show magnifications in the middle graph A. The original differential interferograms 1.b and 2.b have a perpendicular baseline of 191 m and a temporal baseline of 735 d. 1.c and 2.c show interferograms after DEM error correction. The gray areas with very low coherence are set to 0.

Figure S4 shows the profile of the DEM errors and elevation; two magnifications (1 and 2 in Figure S4) show the DEM error maps and an example of an interferogram at 735 d with a perpendicular baseline around 191 m. Thin linear orographic structures were efficiently extracted from the DEM error maps. Figure S4 demonstrates that DEM errors are larger in the presence of steep topography, and display typical oblique

striations at short wavelengths near the edges of sedimentary basins, where the phases are steeper. Sometimes, they exceed half a cycle, making phase unwrapping difficult in these areas. A comparison between the original and corrected differential interferograms shows that most of the residual topographic features were successfully corrected, and the local phase variability was significantly reduced. The correction was set to zero in the grey areas with very low coherence.

The impact of DEM errors on a phase can exceed π, resulting in unwrapping errors of some interferograms in partially incoherent and mountainous areas. Some interferograms with unwrapping errors require visual checking and manual intervention, whereas others can be corrected automatically. For example, Figure S2d is the phase difference of the DEM error-corrected interferogram (Figure S2c) and uncorrected interferogram (Figure S2b). Profile e (Figure S3) shows the values represented by the two colors across the ATF near 0 rad and 6.28 rad. That is, DEM error correction can prevent unwrapping errors by decreasing the phase scatter. The data range of DEM errors (Figure S4) was –7.28 m to 9.60 m.

An unwrapping phase error of 2π can be observed between Figure S2b (unwrapping phase after APS correction) and Figure S2c (unwrapping phase after DEM error correction based on Figure S2b). In Figure S3, profile d is the result of Profile b (from Figure S2b) after subtracting Profile c (from Figure S2c). The straight line with a value of 2π (Figure S3 profile d) demonstrates that the unwrapping errors cross the ATF. After correcting the DEM error, a correct displacement pattern is revealed in Figure S2f and profile f in Figure S3. The results indicate that DEM error correction before the unwrapping step can prevent unwrapping errors in steep topographic areas. Simultaneously, DEM error correction significantly reduces the noise in the wrapped phase for further processing.
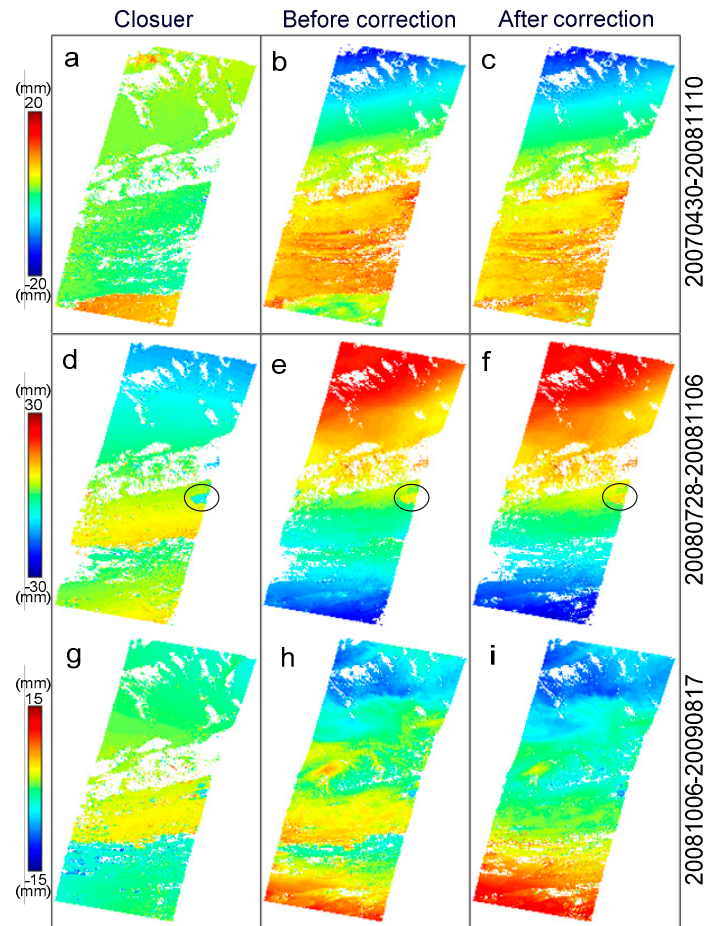
Figure S5. Unwrapping errors detected by a phase-closure technique [58]. (a, d, g) unwrapping errors identified by summing round a loop. (b, e, h) interferograms with unwrapping errors. (c, f, i) corrected interferograms manually.
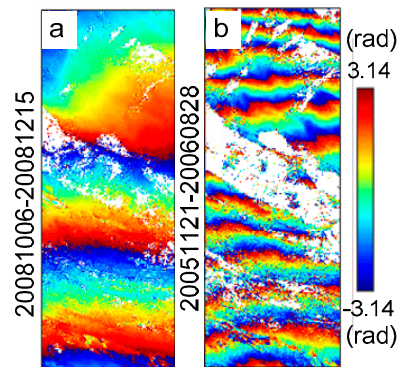

Figure S6. Orbital ramps

Orbital ramp cycles remained in the interferograms (Figure S6). In the orbital error-corrected interferograms (Figures S2e and S2f), the phase ramps were removed respectively from the APS-corrected interferogram (Figure S2b) and the DEM error-corrected interferogram (Figure S2c) after the network orbital correction. Profile e (Figure S3) indicates that the displacement pattern was incorrect; this contradicts the displacement pattern in Profile f (Figure S3). It proves that correcting DEM errors is helpful for areas with steep topography.